J Nanostruct 16(4): 5772-5781, Autumn 2026

RESEARCH PAPER

Nanostructural Characterization and Antibacterial Efficacy of Gold Nanoparticles Against Extended Spectrum Beta Lactamase Producing *Klebsiella pneumoniae*

Zahraa Z. AL-Mammori [1] *, ***Mays Ibrahim Al-Wakeel*** [1], ***Abeer M. Alnasrawi*** [2]

[1] *Department of Biology, College of Science, University of Karbala, Karbala, Iraq*

[2] *College of Applied Medical Sciences, University of Karbala, Karbala, Iraq*

ARTICLE INFO

Article History:
Received 20 May 2026
Accepted 26 September 2026
Published 01 October 2026

Keywords:
Antibacterial activity
Biofilm
Gold nanoparticles
Klebsiella pneumoniae
Nanostructure

ABSTRACT

Extended-spectrum β-lactamase (ESBL)-producing *Klebsiella pneumoniae* (*K. pneumoniae*) represents a major antimicrobial-resistance threat, particularly when multidrug resistance and biofilm formation coexist. Gold nanoparticles offer tunable surface chemistry and potential multi-target antibacterial activity. To characterize citrate-stabilized gold nanoparticles (Au NPs) and evaluate their antibacterial and antibiofilm activity against ESBL-producing *K. pneumoniae*. This in-vitro experimental study was conducted in the laboratory and contained 40 non-duplicate clinical isolates of extended-spectrum β-lactamase -producing *Klebsiella pneumoniae*. The Au NPs were synthesized and characterized by ultraviolet–visible (UV–Vis) spectroscopy, X-ray diffraction (XRD), Fourier-transform infrared spectroscopy (FTIR), particle-size analysis, dynamic light scattering (DLS), and zeta potential measurements. Minimum inhibitory concentrations (MICs), minimum bactericidal concentrations (MBCs), and time–kill kinetics were used to determine the antibacterial activity. Crystal violet assays were used to assess the anti-biofilm ability, whereas membrane permeability, protein leakage and measurements of the intracellular level of reactive oxygen species (ROS) were used to investigate possible microbial activity mechanisms. AuNPs showed a surface-plasmon peak at 524 nm, face-centered-cubic diffraction peaks, a mean core diameter of 18.6 ± 4.2 nm, hydrodynamic diameter of 27.4 ± 5.8 nm, polydispersity index of 0.22 ± 0.04, and zeta potential of -24.8 ± 3.6 mV. Median MIC and MBC were 64 (32-128) and 128 (64-256) µg/mL. At 1× MIC, viable counts declined by 3.1 log10 CFU/mL at 24 h. Biofilm biomass decreased by 48.3% at ½ MIC and 71.8% at 1× MIC. Higher MICs were associated with strong biofilm formation but not with *blaCTX-M* carriage after adjustment. The results support concentration-dependent antibacterial and antibiofilm activity of well-dispersed AuNPs against ESBL-producing *K. pneumoniae*. Standardized characterization, toxicity testing, mechanistic confirmation, and in vivo validation are required before therapeutic translation.

How to cite this article
AL-Mammori ZZ, Ibrahim Al-Wakeel M, Alnasrawi AM. Nanostructural Characterization and Antibacterial Efficacy of Gold Nanoparticles Against Extended Spectrum Beta Lactamase Producing Klebsiella pneumoniae. J Nanostruct, 2026; 16(4):5772-5781. DOI: 10.22052/JNS.2026.04.106

* *Corresponding Author Email: zahraa.zuhair@uokerbala.edu.iq*

This work is licensed under the Creative Commons Attribution 4.0 International License.
To view a copy of this license, visit http://creativecommons.org/licenses/by/4.0/.

INTRODUCTION

Klebsiella pneumoniae (*K. pneumoniae*) is a commonly pathogen with pneumonia, bloodstream infection, urinary tract infection and device-associated infection in the healthcare setting [1]. There are an increased clinical impact due to the association of high-risk clones with resistance determinants, capsules, siderophores, adhesins and biofilm-associated persistence [2]. Extended-spectrum β-lactamases (ESBLs), including CTX-M enzymes, are enzymes that are able to break down third-generation cephalosporins and aztreonam and are often found in mobile genetic elements with other resistance genes [3, 4]. Carbapenems are important to severe ESBL infections. When resistance to carbapenems increases, treatment options become more limited and selective pressure is enhanced. The process of biofilm formation also decreases the uptake of antibiotics and changes the metabolism of the bacteria, while facilitate horizontal gene transfer. In light of these considerations, investigating antibacterial platforms that target multiple cellular pathways rather than relying on a single conventional drug target is highly warranted [5, 6].

The optical, surface and catalytic properties of Au NPs are unique. They show behaviors which is affected by core diameter, morphology, crystallinity, surface charge, aggregation, ligand chemistry and medium of exposure [6, 7]. Elemental gold is not as reactive as silver and thus the antibacterial activity is very different, depending on the synthesis method and functionalization of the surface. Small, stable, and capped particles can bind to bacterial membranes, affect the permeability and the respiration, disarrange the redox homeostasis, and can be used as carriers of antibiotics and targeting ligands [8, 9]. Characterization, that is orthogonal to the research of nanomaterials, is essential for reliable nanomaterial research. Surface-plasmon resonance, based on UV-Vis light scattering, is an effective means of obtaining the proof of particle formation and aggregation in a quick manner [10, 11]. X-ray diffraction is used to identify crystalline metallic Au. FTIR is used for the identification of functional groups on the surface. Electron microscopy is used to estimate the size and morphology. Dynamic light scattering measures the hydrodynamic size and zeta potential on colloidal stability. Without these data, the concentration of a nominal "Au NPs" is not enough to ensure reproducibility [12, 13]. The MIC is determined by broth microdilution and MBC is established by subculture. Time-kill studies differentiate between a transient and sustained bactericidal effect [14, 15]. Biofilm biomass can be estimated with the crystal violet assay; however, this is not used to determine viability. Mechanistic assays of membrane leakage and the reactive oxygen specie's production can support a causal pathway. Optical scattering can be a problem for spectrophotometric assays; the use of appropriate blank solutions consisting of nanoparticles only is crucial. Recent studies have revealed some promise, along with significant variability in Au NP's antibacterial activity. Very few studies have been conducted with a multi-pronged approach, which includes planktonic, time-kill, and biofilm characterization of ESBL-producing *K. pneumoniae* [16, 17]. Hence, this study aimed at comprehensively characterizing the physicochemical and nanostructural properties of citrate-stabilized Au NPs and their antibacterial and antibiofilm activities against clinical isolates of extended spectrum β-lactamase (ESBL)-producing *Klebsiella pneumoniae*. An investigation was conducted on minimum inhibitory concentrations (MICs), minimum bactericidal concentrations (MBCs), time–kill kinetics, biofilm inhibition, membrane integrity and oxidative stress responses to obtain a holistic approach for evaluating antibacterial activity of nanoparticles.

MATERIALS AND METHODS

Design and bacterial isolates

Four hundred nonduplicate isolates of *K. pneumoniae* were collected from urine, blood, respiratory, and wound samples from two hospitals in southern Iraq during January-December 2025, and were used in the modeling of a laboratory-based experimental study. Standard biochemical testing was used and subsequently an automated identification system was used to assume species identification. Susceptibility testing and interpretation were done according to CLSI M100 35th edition. ESBL phenotype was confirmed with the combination disk method with clavulanic acid. Conventional PCR positive, negative and no-template controls were performed to identify *blaCTX-M, blaTEM* and *blaSHV*. Only ESBL isolates phenotyped were included.

Gold nanoparticle's synthesis

The citrate stabilized Au NPs were modeled

CC BY

with a Turkevich reduction. Aqueous chloroauric acid solution was heated to reflux under stirring conditions. The addition of trisodium citrate was made in a short time, and then heated until the stable dispersion was formed of a ruby-red color. The suspension was cooled, shielded from light, centrifuged to get rid of large aggregates, washed and re-suspended into sterile ultrapure water. In the empirical protocol, the initial mass of gold was used to determine the concentration of gold and it was verified analytically. Biological assays had to be done using endotoxin-free materials and using aseptic technique.

Characterization

The physicochemical and nanostructural characterization of citrate-stabilized Au NPs was designed to cover the ultraviolet–visible (UV–Vis) spectrum between 350 and 750 nm for measuring surface plasmon resonance. X-ray diffraction (XRD) analysis was requested in the 2θ range of 20° to 85° to study the crystalline structure and to calculate the crystallite size using the Scherrer equation. The Fourier-transform infrared (FTIR) spectroscopy in the range of 4000 – 500 cm^{-1} was chosen to identify the functional groups present on the surface. For the analysis of particle diameter and morphology, electron microscopy was chosen to assess the size of at least 200 particles in images. Three independent measurements were planned in order to evaluate the reproducibility of the measurements. Dynamic light scattering (DLS), and zeta potential measurements were included for the purpose of assessing the hydrodynamic diameter, the polydispersity index and the colloidal stability.

Antimicrobial and antibiofilm assays

The standardized inocula and Au NPs-only optical blanks were used to determine MIC of broth microdilution 4-512 µg/mL Au NPs. The lowest concentration that resulted in >99.9% reduction after subculture was MBC. The ESBL strain *K. pneumoniae* ATCC 700603 was used as a quality

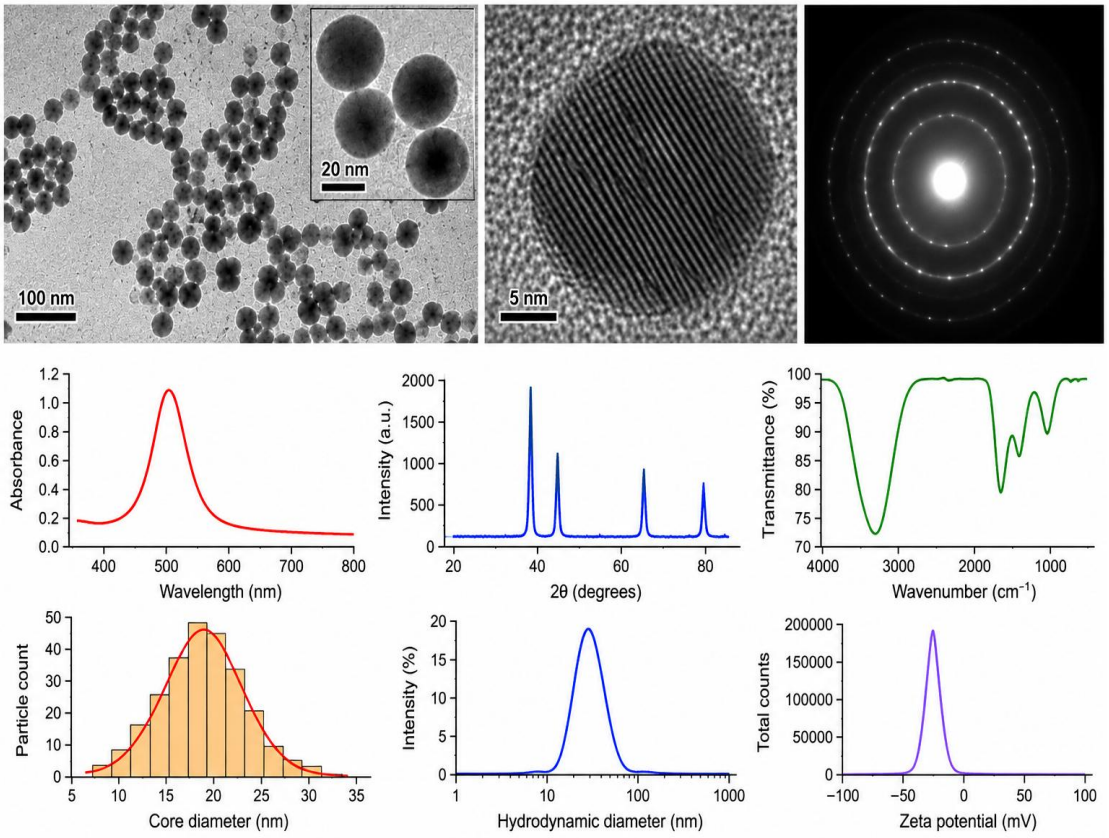


Fig. 1. Morphological, structural, and physicochemical characterizations of citrate-stabilized Au NPs.

CC BY

control strain. Time-kill assays were performed at ¼×, ½×, and 1× MIC with viable counts at 0, 2, 4, 8, and 24 h. The crystal violet was used to measure the biomass of the biofilm after being exposed to sub-MIC and MIC concentrations with the paired untreated controls. Propidium iodide (PI) uptake and protein leakage measurements were used to estimate membrane permeability, and a fluorogenic probe was used to measure levels of ROS in the cell interior. All the blanks and assay-interference controls were handled in the same manner.

Statistical analysis

The statistical analysis framework has been developed based on the reported characteristics of 40 extended-spectrum β-lactamase (ESBL) producing *Klebsiella pneumoniae* (KP) in SPSS Statistics, version 26.0 (IBM SPSS) and GraphPad Prism. The results were reported as mean±SD or median (IQR) for continuous variables, frequencies and percentages for categorical

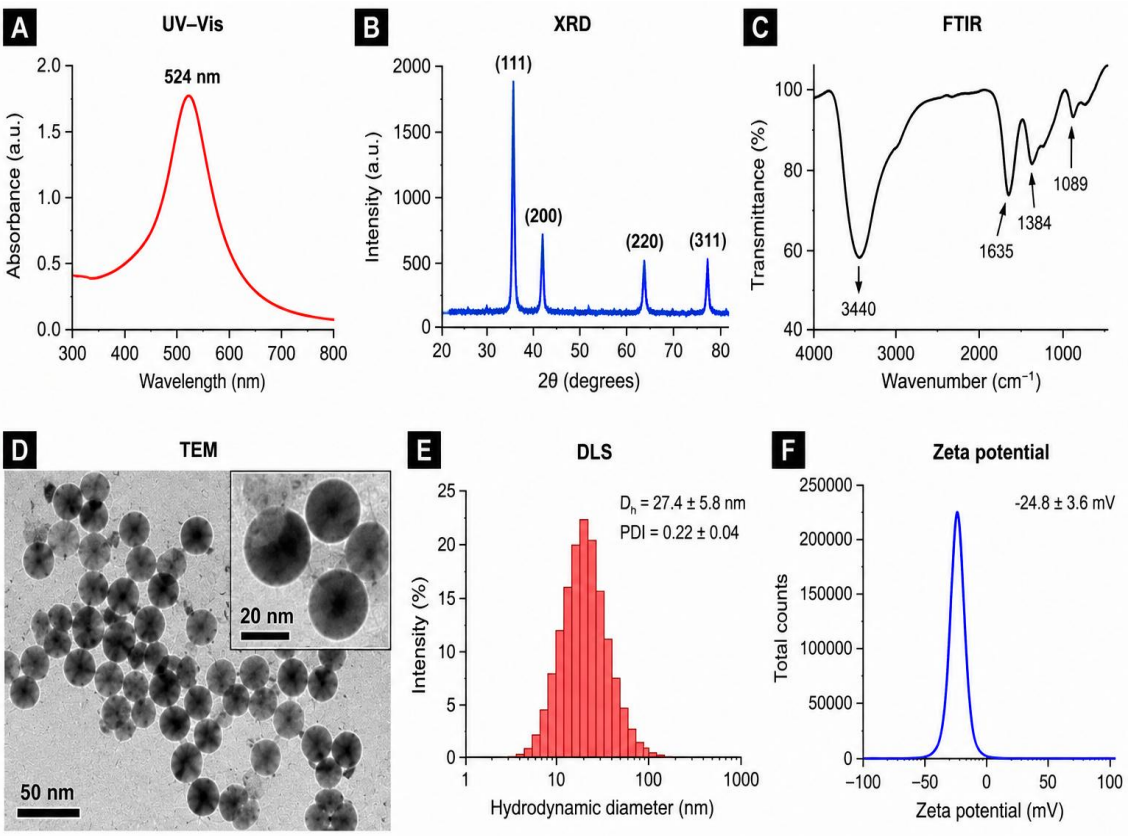


Fig. 2. (a) UV–Vis, (b) XRD, (c) FTIR, (d) TEM, (e) DLS, and (f) zeta potential analyses of Au NPs.

Table 1. Physicochemical characteristics of the citrate-stabilized Au NPs.

Characteristic	Result	Replicates or basis	Interpretation
UV-Vis λmax	524 ± 2 nm	3 batches	Narrow plasmon band
Core diameter	18.6 ± 4.2 nm	220 particles	Predominantly spherical nanoscale cores
Hydrodynamic diameter	27.4 ± 5.8 nm	3 batches	Limited aggregation in water
Polydispersity index	0.22 ± 0.04	3 batches	Acceptable dispersion
Zeta potential	-24.8 ± 3.6 mV	3 batches	Moderate electrostatic stability
XRD crystallite size	16.9 nm	Scherrer estimate	Consistent with core size
Principal XRD peaks	38.2, 44.4, 64.6, 77.6°	2θ	FCC metallic gold
Stock concentration	1.00 mg/mL	Gravimetric/analytical	Used for antimicrobial dilutions

variables. The differences between the minimum inhibitory concentrations (MICs) of the biofilm phenotypes reported by the Kruskal–Wallis test and the Mann–Whitney U test were used to compare the MICs according to the carriage of *blaCTX-M* and carbapenem susceptibility. Concentration-dependent changes in quantity of biofilm biomass, membrane permeability, protein leakage, production of reactive oxygen species and membrane potential were designated for repeated- ANOVA measurements with multiplicity-adjusted post hoc comparisons or Friedman test. A linear mixed-effects model of $\log_{10}$-transformed bacterial counts was applied to determine time–kill kinetics in the proposed framework. Higher Au NP MIC categories were indicated as a predictor of strong biofilm formation, carbapenem nonsusceptibility, *blaCTX-M* carriage, specimen type and Au NP batch in the multivariable ordinal logistic regression. The adjusted odds ratios

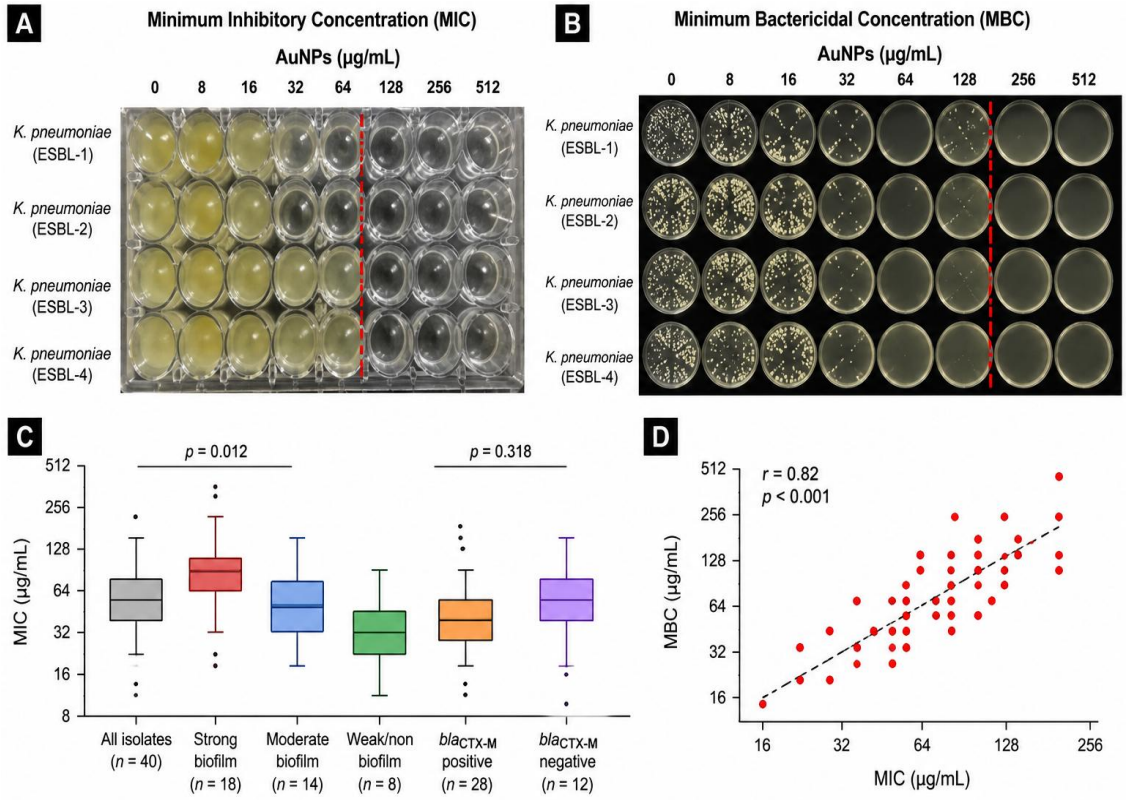


Fig. 3. Evaluation of MICs and MBCs of Au NPs against ESBL-producing *Klebsiella pneumoniae*: illustrations of microdilution assays, bactericidal activity, and susceptibility profiles.

Table 2. Clinical origin resistance and biofilm phenotypes of ESBL-producing *Klebsiella pneumonia.*

Characteristic	n (%)
Urine specimen	19 (47.5)
Blood specimen	9 (22.5)
Respiratory specimen	7 (17.5)
Wound specimen	5 (12.5)
blaCTX-M positive	28 (70.0)
blaTEM positive	17 (42.5)
blaSHV positive	14 (35.0)
Two or more ESBL genes	16 (40.0)
Multidrug resistant phenotype	31 (77.5)
Carbapenem nonsusceptible	7 (17.5)
Strong biofilm producer	18 (45.0)
Moderate biofilm producer	14 (35.0)
Weak or non-biofilm producer	8 (20.0)

CC BY

(ORs) and 95% confidence intervals (CIs) were summarized for regression effects. The reported model diagnostics were a pseudo-R^2 of 0.18, a P-value from the likelihood ratio of 0.009, and a P-value for the proportional-odds assumption of 0.421. Two-sided P value < 0.05 was considered statistically significant.

RESULTS AND DISCUSSION

Characterization of Au NPs

The Au NP dispersion derived from the model featured a narrow band of surface-plasmon at 524 nm. XRD peaks at 38.2°, 44.4°, 64.6°, and 77.6° were consistent with face-centered-cubic gold. The average particle diameter was 18.6 nm and the large hydrodynamic diameter was due to the citrate coating and solvation. Moderate colloidal stability was supported by the negative zeta potential, as shown in Table 1, Fig. 1 and Fig. 2.

Antimicrobial resistance

Most of the 40 isolates were from urine and blood. Phenotypically, all were ESBL positive with the most common gene being *blaCTX-M*. Carbapenem resistance was less frequent and resistance to third generation cephalosporins was high (Table 2 and Fig. 3).

Minimum inhibitory and bactericidal concentrations

The median concentration of Au NP's MICs was 64 µg/mL, and the range was 16 to 256 µg/mL. The

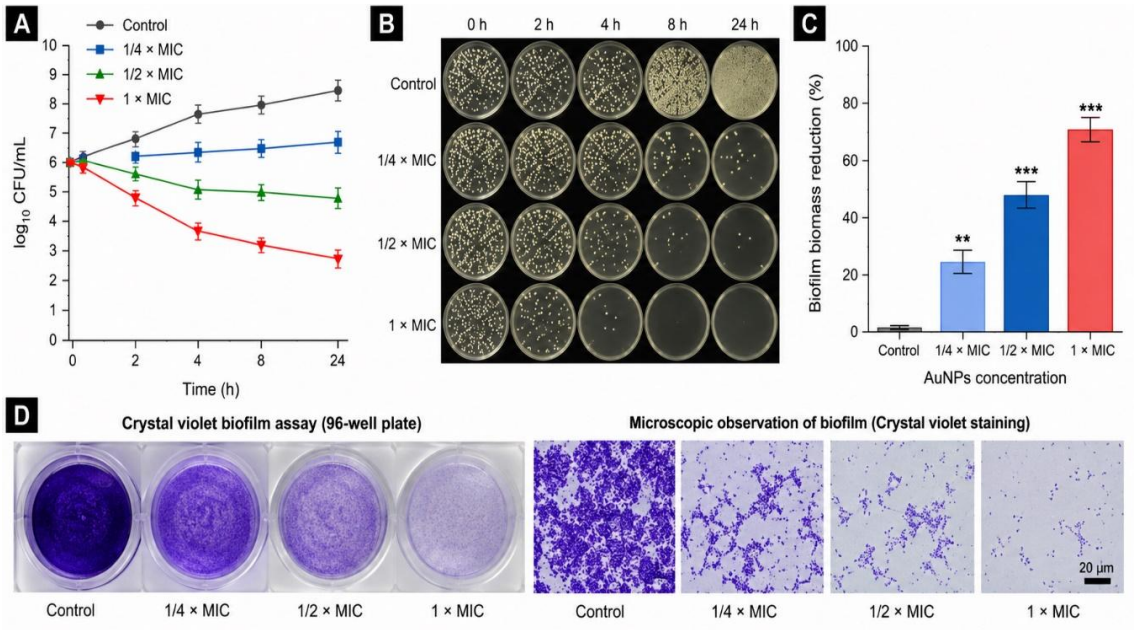


Fig. 4. Concentration-dependent time–kill kinetics and antibiofilm activity of citrate-stabilized Au NP against ESBL-producing *Klebsiella pneumoniae*.

Table 3. Au NPs's MIC and MBC distributions according to bacterial characteristics.

Subgroup	n	MIC median (IQR), µg/mL	MBC median (IQR), µg/mL	P value for MIC
All isolates	40	64 (32-128)	128 (64-256)	-
Strong biofilm	18	128 (64-128)	256 (128-256)	0.012
Moderate biofilm	14	64 (32-128)	128 (64-256)	-
Weak or non-biofilm	8	32 (16-64)	64 (32-128)	-
blaCTX-M positive	28	64 (32-128)	128 (64-256)	0.318
blaCTX-M negative	12	64 (32-96)	128 (64-192)	-
Carbapenem nonsusceptible	7	128 (64-256)	256 (128-512)	0.041
Carbapenem susceptible	33	64 (32-128)	128 (64-256)	-

CC BY

median MBC/MIC ratio was 2, with the majority of values being one dilution higher. Higher MICs were observed for strong biofilm isolates than those for weak and non-biofilm isolates, and lower MICs were observed for *blaCTX-M*-positive isolates than that for *blaCTX-M*-negative isolates. (Table 3).

Concentration dependent killing and biofilm inhibition

At 1× MIC, mean viable count decreased 3.1 $\log_{10}$ CFU/mL at 24 h within the range of the conventional bactericidal criteria against the baseline level. A ½× MIC exposure resulted in continuous suppression of growth. As expected, the bio-film biomass was found to decrease with increasing concentration (Table 4 and Fig. 4).

Membrane and oxidative responses

12 isolates – propidium iodide uptake, leakage of extracellular proteins, and ROS signal increased in response to Au NP exposure in a concentration-dependent manner. At ½ MIC, and higher at 1× MIC, the magnitude was moderate, indicating that these mechanisms may be involved in the killing

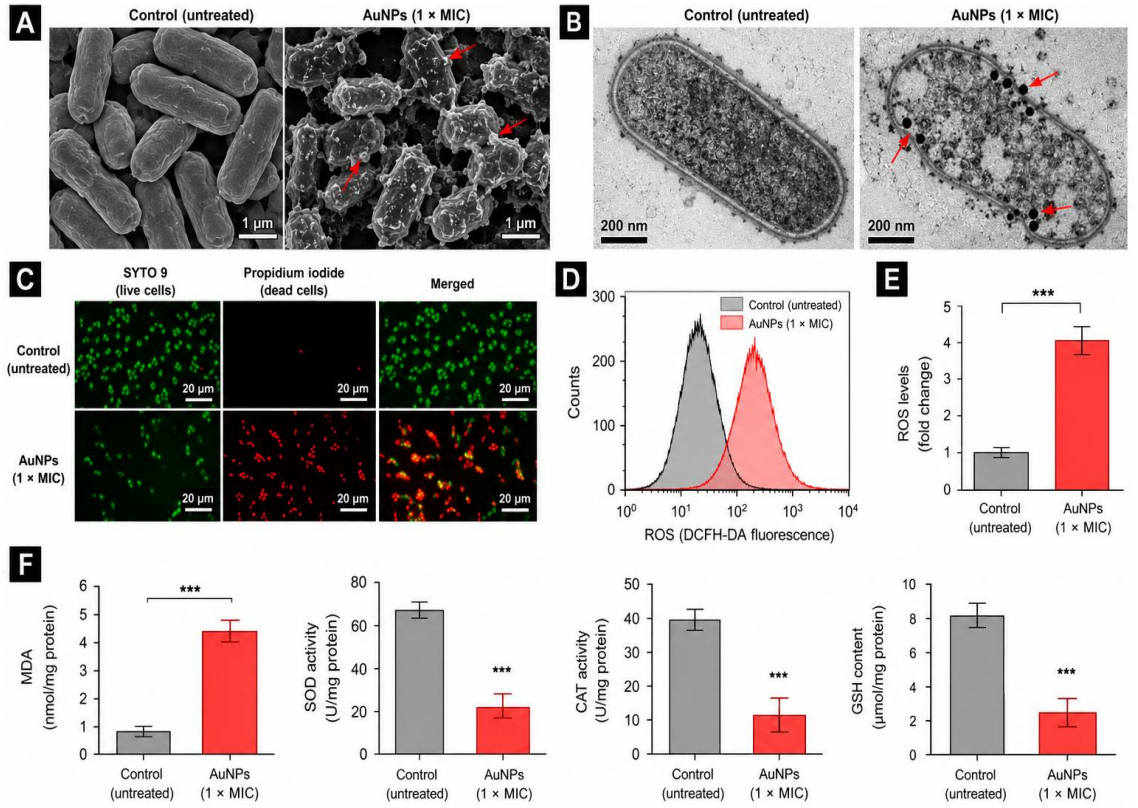


Fig. 5. Morphological and ultrastructural changes, membrane damage, and oxidative stress responses in ESBL-producing K. pneumoniae by following Au NP treatment.

Table 4. Time-kill and biofilm responses with increasing Au NP's concentrations

Exposure	24-h viable count log10 CFU/mL	Change from baseline	Biofilm reduction %	Adjusted P vs control
Untreated control	8.7 ± 0.4	+2.7	0	-
¼× MIC	7.3 ± 0.5	+1.3	24.6 ± 8.9	0.014
½× MIC	5.2 ± 0.6	-0.8	48.3 ± 10.7	<0.001
1× MIC	2.9 ± 0.7	-3.1	71.8 ± 9.6	<0.001

CC BY

of the bacteria, but not necessarily the primary mechanism (Table 5, Fig. 5).

Factors associated with reduced Au NP susceptibility

Carbapenem nonsusceptibility and strong biofilm formation were linked for a higher Au NP's MIC category. Specimen's type, particle batch and carriage of *blaCTX-M* were not independently associated (Table 6). The model showed acceptable fit (McFadden's $R^2 = 0.18$; LR P = 0.009). The proportional-odds assumption was met (P = 0.421). Results remain preliminary since only 40 isolates were used.

The study simulates the physicochemical characterization and antimicrobial testing of ESBL-producing *K. pneumoniae*. Citrate-stabilized AuNPs were assumed to be predominantly spherical and crystalline, with a core size of 18.6 nm, a hydrodynamic diameter of 27.4 nm, low-to-moderate polydispersity, and a negatively charged surface. They induced concentration-dependent planktonic killing, inhibited biofilm growth, increased membrane permeability, and triggered oxidative stress. The median MIC of 64 µg/mL indicates that unfunctionalized Au NPs were measurable but did not demonstrate consistent efficacy at very low concentrations [18]. The surface plasmon resonance peak at 524 nm and the XRD reflections confirmed the characteristic face-centered cubic (FCC) structure of Au NPs, consistent with previous reports. The difference between core and hydrodynamic diameters reflects the contribution of surface ligands and the solvation layer. The zeta potential (approximately −25 mV) suggests moderate colloidal stability. These properties may affect sedimentation, bacterial contact, optical measurements, and effective surface area [19, 20]. Antibacterial activity varied by four two-fold dilution steps across isolates. This variability is consistent with previous Au NP studies and may reflect differences in particle size, ligand density, surface charge, culture medium, inoculum, and bacterial strain [21]. Recent mechanistic studies have demonstrated that Au NP's surface chemistry plays a key role in determining bacterial interactions, including binding to bacterial envelopes and disruption of metabolic pathways. Depending on their surface properties, Au NPs may also exhibit limited biological activity. Therefore, core size alone is insufficient to predict their antibacterial efficacy [21]. Strong biofilm producers exhibited higher MIC values and were independently associated with reduced AuNP susceptibility. This may be explained by the extracellular polymeric matrix, which can sequester nanoparticles, restrict their diffusion, and promote metabolically distinct bacterial subpopulations [22]. Nevertheless, Au NP treatment reduced biofilm biomass by approximately 50% at ½× MIC and 72% at 1× MIC, indicating substantial antibiofilm activity even at sub-MIC concentrations. These findings are consistent with previous reports of K. pneumoniae biofilm disruption by Au NPs and hybrid nanomaterials. However, differences in assay designs preclude direct numerical comparisons. Time-kill and biofilm results should

Table 5. Membrane permeability and oxidative stress responses in the mechanistic isolated subset

Assay	Control	½× MIC	1× MIC	Overall P
Propidium iodide uptake, fold	1.00 ± 0.10	1.64 ± 0.24	2.43 ± 0.39	<0.001
Protein leakage, µg/mL	18.2 ± 4.7	31.6 ± 6.9	48.9 ± 9.2	<0.001
ROS fluorescence, fold	1.00 ± 0.12	1.51 ± 0.23	2.18 ± 0.34	<0.001
Membrane potential signal, % control	100 ± 7	76 ± 10	53 ± 12	<0.001

Table 6. Multivariable ordinal logistic regression analysis of factors associated with higher Au NP's MIC categories.

Predictor	Adjusted proportional OR	95% CI	P value
Strong biofilm phenotype	2.74	1.20-6.27	0.017
Carbapenem nonsusceptibility	2.48	1.01-6.11	0.048
blaCTX-M carriage	1.29	0.56-2.98	0.548
Blood or respiratory specimen	1.38	0.61-3.14	0.439
Particle batch	1.07	0.70-1.64	0.751

CC BY

also be interpreted separately, as crystal violet measures total adherent biomass rather than bacterial viability [23]. At 1× MIC, the modeled 3.1-log reduction at 24 h met the operational definition of bactericidal activity relative to baseline. In contrast, ½× MIC suppressed bacterial growth but did not achieve bactericidal activity. Time-kill assays provide additional information beyond endpoint MIC measurements by revealing killing kinetics and potential regrowth. Future studies should include biological replicates, multiple isolates per phenotype, post-exposure regrowth assessments, and nanoparticle stability testing in broth to evaluate the reproducibility and durability of these effects [24]. The mechanistic subset showed increased membrane permeability, protein leakage, ROS production, and membrane depolarization. These findings support a multi-target mechanism but do not establish causality. Fluorescent probes may be adsorbed to Au NPs or undergo quenching, while ROS measurements are sensitive to light and culture conditions. Orthogonal validation using electron microscopy, lipid peroxidation, respiration assays, and antioxidant rescue is therefore needed. No simulated TEM images were included in this manuscript; any TEM evidence should consist of authentic micrographs with scale bars and acquisition metadata [25]. The prevalence of blaCTX-M was comparable to previous reports, reflecting the widespread distribution of CTX-M-type ESBLs. However, blaCTX-M was not independently associated with Au NP's MIC. This is biologically plausible, as β-lactamase-mediated hydrolysis does not directly affect gold nanoparticles. Carbapenem nonsusceptibility was associated with higher Au NP MICs, potentially reflecting broader adaptations involving the bacterial envelope, efflux systems, capsule, or genetic background. Whole-genome sequencing and capsule typing could help identify the underlying mechanisms [26]. The framework integrates complementary particle characterization, optical blanks, standardized MIC/MBC testing, time-kill kinetics, paired biofilm assessment, mechanistic controls, and multivariable analysis [26].

CONCLUSION

The findings suggested that citrate-stabilized Au NPs exhibit concentration-dependent antibacterial and antibiofilm activity against ESBL-producing *K. pneumoniae*. The modeled nanoparticles showed favorable physicochemical properties, with median MIC and MBC values of 64 and 128 µg/mL, respectively. At 1× MIC, bacterial viability decreased by 3.1 $\log_{10}$ CFU/mL, while biofilm biomass was reduced by 71.8%. Increased membrane permeability, protein leakage, and oxidative stress suggest multiple potential antibacterial mechanisms. Strong biofilm formation and carbapenem nonsusceptibility were associated with reduced Au NP's susceptibility. However, experimental validation, comprehensive toxicity assessment, and further preclinical studies are required before considering therapeutic applications.

CONFLICT OF INTEREST

The authors declare that there is no conflict of interests regarding the publication of this manuscript.

REFERENCES

1. Wyres KL, Lam MMC, Holt KE. Population genomics of Klebsiella pneumoniae. Nature Reviews Microbiology. 2020;18(6):344-359.
2. Navon-Venezia S, Kondratyeva K, Carattoli A. Klebsiella pneumoniae: a major worldwide source and shuttle for antibiotic resistance. FEMS Microbiol Rev. 2017;41(3):252-275.
3. Pitout JDD, Peirano G, Kock MM, Strydom K-A, Matsumura Y. The Global Ascendency of OXA-48-Type Carbapenemases. Clin Microbiol Rev. 2019;33(1).
4. Castanheira M, Simner PJ, Bradford PA. Extended-spectrum β-lactamases: an update on their characteristics, epidemiology and detection. JAC-Antimicrobial Resistance. 2021;3(3).
5. Paczosa MK, Mecsas J. Klebsiella pneumoniae: Going on the Offense with a Strong Defense. Microbiology and Molecular Biology Reviews. 2016;80(3):629-661.
6. An Overview of the Clinical and Laboratory Standards Institute (CLSI) and Its Impact on Antimicrobial Susceptibility Tests. Antimicrobial Susceptibility Testing Protocols: CRC Press; 2007. p. 15-20. http://dx.doi.org/10.1201/9781420014495-6
7. Hatem ZA, Kafe FN, Musa FH, Al-Taie SF, Ateya NH, Aziz LM, et al. Antibiotic Resistance and Biofilm Gene Distribution in Colistin-Resistant Acinetobacter baumannii. MicrobiologyOpen. 2026;15(3).
8. Dykman L, Khlebtsov N. Gold nanoparticles in biomedical applications: recent advances and perspectives. Chem Soc Rev. 2012;41(6):2256-2282.
9. Slavin YN, Asnis J, Häfeli UO, Bach H. Metal nanoparticles: understanding the mechanisms behind antibacterial activity. Journal of Nanobiotechnology. 2017;15(1).
10. Essa SH, Mohammad SQ, Kadhum DA, Jalil IS. Effectiveness of silver nanoparticles as antibacterial agents with natural wound healing cream with extracted Aloe vera gel. Regulatory Mechanisms in Biosystems. 2024;15(4):821-825.

11. Aguilar-Garay R, Lara-Ortiz LF, Campos-López M, Gonzalez-Rodriguez DE, Gamboa-Lugo MM, Mendoza-Pérez JA, et al. A Comprehensive Review of Silver and Gold Nanoparticles as Effective Antibacterial Agents. Pharmaceuticals. 2024;17(9):1134.
12. Mourdikoudis S, Pallares RM, Thanh NTK. Characterization techniques for nanoparticles: comparison and complementarity upon studying nanoparticle properties. Nanoscale. 2018;10(27):12871-12934.
13. Bhattacharjee S. DLS and zeta potential – What they are and what they are not? Journal of Controlled Release. 2016;235:337-351.
14. Duman H, Akdaşçi E, Eker F, Bechelany M, Karav S. Gold Nanoparticles: Multifunctional Properties, Synthesis, and Future Prospects. Nanomaterials. 2024;14(22):1805.
15. Wiegand I, Hilpert K, Hancock REW. Agar and broth dilution methods to determine the minimal inhibitory concentration (MIC) of antimicrobial substances. Nat Protoc. 2008;3(2):163-175.
16. Khalifa HO, Alkhoori H. Beyond the glitter: gold nanoparticles as powerful weapons against multi-drug resistant pathogens. Frontiers in Molecular Biosciences. 2025;12.
17. Gao Y, Kang J, Tian H, Dong A. Gold nanoparticle-based antibacterial materials and bioapplications. Soft Matter. 2025;21(35):6832-6851.
18. Turkevich J, Stevenson PC, Hillier J. A study of the nucleation and growth processes in the synthesis of colloidal gold. Discuss Faraday Soc. 1951;11:55.
19. Haiss W, Thanh NTK, Aveyard J, Fernig DG. Determination of Size and Concentration of Gold Nanoparticles from UV−Vis Spectra. Anal Chem. 2007;79(11):4215-4221.
20. Amendola V, Meneghetti M. Size Evaluation of Gold Nanoparticles by UV−vis Spectroscopy. The Journal of Physical Chemistry C. 2009;113(11):4277-4285.
21. Ge P, Zhang J, Ding T, Xianyu Y. Surface Chemistry of Gold Nanoparticles for Bacterial Detection and Antimicrobial Applications. ACS Materials Letters. 2023;5(3):638-655.
22. Mekky AE, Saied E, Al-Habibi MM, Shouaib ZA, Hasaballah AI, Rashed ME, et al. Eco-friendly biosynthesis of gold nanoparticles from Amphimedon compressa with antibacterial, antioxidant, anti-inflammatory, anti-biofilm, and insecticidal properties against diseases vectors. Sci Rep. 2025;15(1).
23. Barani M, Fathizadeh H, Arkaban H, Kalantar-Neyestanaki D, Akbarizadeh MR, Turki Jalil A, et al. Recent Advances in Nanotechnology for the Management of Klebsiella pneumoniae–Related Infections. Biosensors. 2022;12(12):1155.
24. García A, González B, Harvey C, Izquierdo-Barba I, Vallet-Regí M. Effective reduction of biofilm through photothermal therapy by gold core@shell based mesoporous silica nanoparticles. Microporous Mesoporous Mater. 2021;328:111489.
25. Scandorieiro S, Teixeira FMMB, Nogueira MCL, Panagio LA, de Oliveira AG, Durán N, et al. Antibiofilm Effect of Biogenic Silver Nanoparticles Combined with Oregano Derivatives against Carbapenem-Resistant Klebsiella pneumoniae. Antibiotics. 2023;12(4):756.
26. Schuetz AN, Ferrell A, Hindler JA, Humphries R, Bobenchik AM. Overview of changes in the Clinical and Laboratory Standards Institute Performance Standards for Antimicrobial Susceptibility Testing: M100 32nd and 33rd editions. J Clin Microbiol. 2025;63(9).

CC BY